31st Annual International Conference of the IEEE EMBS
Minneapolis, Minnesota, USA, September 2-6, 2009

Pulsed Magneto-Acoustic Imaging

Mohammad Mehrmohammadi, Junghwan Oh, Salavat R. Aglyamov, Andrei B. Karpiouk,
Stanislav Y. Emelianov, *Member, IEEE*

Abstract— **Nanoparticles are attracting considerable interest as contrast agents for many different imaging modalities. Moreover, imaging the events at the cellular and molecular level is possible by using nanoparticles that have the desired targeting moiety. Unfortunately, ultrasound imaging cannot visualize the nano-structures directly due to its limited spatial resolution and contrast. We present a new technique, pulsed magneto-acoustic imaging, capable of imaging magnetic nanoparticles indirectly. In this method, a high-strength pulsed magnetic field is used to induce motion within the magnetically labeled tissue and ultrasound is used to detect internal tissue motion. Experiments on tissue-mimicking phantoms and ex-vivo animal tissues demonstrated a clear contrast between normal and iron-laden samples labeled with 5 nm magnetic nanoparticles. In addition, the sensitivity of this new imaging technique was investigated for different concentrations of magnetic agents. The results of the study suggest that magnetic nanoparticles can be used as contrast agents in pulsed magneto-acoustic imaging. Furthermore, PMA imaging could become an imaging tool capable of visualizing the cellular and molecular composition of deep-lying structures.**

I. Introduction

Ultrasound is one of the most widely used imaging modalities due to its specific features such as non-ionization, real time, reliability and cost effectiveness. However, ultrasound imaging cannot visualize the events at molecular and cellular levels because of its limited spatial resolution and contrast. Therefore, contrast agents have been introduced to enhance and improve the quality of ultrasound images [1]. Besides improving the general contrast of the imaging system, an ideal contrast agent needs to provide additional information about molecular and cellular content of tissue. Moreover, agents should be injectable intravenously, non-toxic and stable during the imaging procedure. Unfortunately, common ultrasound contrast agents do not fulfill these requirements. For example, microbubbles are too large to cross the microvasculature and bind to specific cells. Microbubbles also have short life spans in the circulation system and may collapse when exposed to ultrasound pressure waves. Nano-scale perfluorocarbon (PFC) and liposome contrast agents cannot produce strong ultrasound reflections and thus create limited contrast in ultrasound images [2, 3].

Metal based nanoparticles are being extensively used as molecular contrast agents for various imaging modalities such as optical imaging and MRI. Because of their small size (<100 nm), they are suitable for molecular and cellular imaging. Molecularly targeted nanoparticles can bind to specific molecular biomarkers and thus provide pathology information at early stages of development [4]. Unfortunately, ultrasound imaging cannot detect the nano-structures directly because of their small size and ultrasound reflectivity.

Previously, we introduced magneto-motive ultrasound (MMUS), capable of imaging magnetic nanoparticles indirectly [5]. MMUS utilizes both a high strength sinusoidal magnetic field to induce motion within the magnetically labeled tissue and ultrasound to detect the internal tissue motion. The induced motion is proportional to the magneto-motive force which is also proportional to magnetic flux density squared [6]. However, a larger magnetic field can generate heat in iron-laden tissue. Indeed, generation of heat in magnetically labeled tissue in the presence of a time-varying magnetic field is one of the possible concerns associated with the safety of MMUS imaging [7]. Consequently, using MMUS to image deeper tissue structures is limited by thermal constraints. To overcome this limitation, we have developed a pulsed magneto-acoustic (PMA) imaging approach that utilizes pulsed magnetic excitation instead of a continuous field while using the same contrast mechanism. In this paper, we investigate the behavior of a magnetic particle in a viscoelastic medium in response to a pulsed magneto-motive force and explore the capabilities of pulsed magneto-acoustic imaging.

II. Behavior of Magnetic Nanoparticles in Response to a Pulsed Magnetic Field

The motion of a magnetic particle is defined by the characteristics of the pulsed magneto-motive force and also the mechanical properties of the surrounding background. In this section, the pulsed magneto-motive force and the behavior of a magnetic particle in response to it will be further investigated.

Manuscript received April 7, 2009. This work was supported in part by the National Institutes of Health under grant EB 008821.

M.M., S.A., A.K. and S.E. are with the Department of Biomedical Engineering, University of Texas at Austin, Austin, TX 78712 USA (phone: 512-471-7520; fax: 512-471-0616; e-mail: emelian@mail.utexas.edu).

J.H.O. was with the Department of Biomedical Engineering, University of Texas at Austin, Austin, TX 78712. He is now with the Department of Mechanical Engineering, Pukyong National University, South Korea.

A. Pulsed magneto-motive force

The magneto-motive force (F_m) acting on a magnetic nanoparticle can be expressed as:

$$F_m = (m \bullet \nabla) B \,, \tag{1}$$

where m is the magnetic moment. Considering a z-directional magnetic flux B=(0,0,B_z), the magnetic moment (m) of paramagnetic nanoparticles can be described as (0,0,m_z). Therefore, the magneto-motive force F_m can be expressed as $F_m = (m_z \bullet \nabla) B_z$. When a magnetic nanoparticle is located in a weakly diamagnetic medium such as tissue, the magnetic moment, m_z can be written as $m_z = V_m M_z$. Here V_m is the volume of the magnetic portion of the nanoparticle and can be denoted as $V_m = V_{np} f_m$ where V_{np} is the total size of the nanoparticle and f_m is a dimensionless factor called fraction of magnetite. This fraction represents the volumetric ratio of magnetic material in a nanoparticle. The z-directional volumetric magnetization M_z can be written as $M_z = (\chi_{np} - \chi_{medium}) H_z$ where H_z is the magnetic field strength in the z-direction, and χ_{np} and χ_{medium} are the susceptibilities of the magnetic nanoparticles and the surrounding medium respectively. The magnetic susceptibility of the medium, i.e., tissue is negligible compared to its value in magnetic nanoparticles. Assuming that B does not change significantly over the nanoparticle due to its small size, the volumetric magnetization M_z can be expressed as $M_z = \chi_{np} \frac{B_z}{\mu_0}$ and, therefore, the magneto-motive force is:

$$F_m = \frac{V_{np} f_m \chi_{np}}{\mu_0} (B_z \bullet \nabla) B_z \,. \tag{2}$$

Where μ_0 is the magnetic constant. Since

$$(B_z \bullet \nabla) B_z = \frac{1}{2} \nabla (B_z \bullet B_z) = B_z \frac{\partial B_z}{\partial z}, \tag{3}$$

Equation (2) can be simplified to:

$$F_m = \frac{V_{np} f_m \chi_{np}}{\mu_0} B_z \frac{\partial B_z}{\partial z} \,. \tag{4}$$

Equation (4) clearly shows that the magneto-motive force depends on the magnetic flux density and its gradient over distance as well as on the magnetic properties of the particles.

B. Motion of an iron-laden inclusion within a viscoelastic medium under pulse excitation

The motion of an incompressible medium can be characterized through the governing equation:

$$-\nabla P + \mu \nabla^2 \bar{U} + \eta \nabla^2 \frac{\partial \bar{U}}{\partial t} = \rho \frac{\partial^2 \bar{U}}{\partial t^2} \tag{5}$$

Where P is the internal pressure, μ and η are shear elasticity and viscosity coefficients, ρ is the medium density, t is time and $\bar{U}$ represents the displacement vector. In a PMA imaging system, nanoparticles experience the magneto-motive force as short pulses (6-10 ms). Therefore, the motion in time domain can be written as:

$$U_z + \frac{R}{c_t} \dot{U}_z + \frac{1}{9}(1+2\beta) \frac{R^2}{c_t^2} \ddot{U}_z = \frac{F_{magneto-motive}(t)}{6\pi\mu R} \tag{6}$$

where U_z is the displacement in z-direction, $F_{magneto-motive}(t)$ is the applied external magneto-motive force, R is the radius of the spherical nanoparticle, $c_t = \sqrt{(\mu/\rho)}$ is the shear wave speed and $\beta = \rho_{NP}/\rho$ is the nanoparticle density (ρ_{NP}) normalized by medium density [8]. The displacement of an iron-laden inclusion inside an incompressible background will be determined by the displacement of all magnetic nanoparticles.

III. Materials and Methods

To demonstrate the ability of the PMA imaging system to detect the magnetic nanocomposites, experiments were performed using tissue-mimicking phantoms and ex-vivo cell-tissue phantoms. In phantom experiments, the sensitivity of the custom-built PMAI system was investigated through imaging tissue-mimicking phantoms with different concentrations of magnetic nanoparticles. In the ex-vivo experiments macrophage cells internalized with magnetic nanoparticles and embedded into tissue background were imaged. In both experiments, FDA approved and commercially available superparamagnetic iron-oxide (SPIO) nanoparticles (Feridex I.V., Bayer Healthcare, Inc.) were used as magnetic contrast agents. These dextran-coated magnetic iron oxide nanoparticles are also used as MRI contrast agents.

A. Tissue mimicking phantoms

Tissue mimicking phantoms were made out of 8% polyvinyl alcohol and different concentrations of magnetic nanoparticles (0.2, 0.5, 1 and 2 mgr Fe per cubic centimeter of mixture) along with a control sample with no magnetic nanoparticles. To obtain better ultrasound images, 0.5% of 15 µm silica nanoparticles were added as ultrasound scatters. All samples were made in a 2 mm diameter tube and went through four 12-hour freeze/thaw cycles.

B. Tissue/cell phantoms

The second set of experiments was performed using mouse kidney tissue injected with magnetically labeled macrophage cells suspended within 10% gelatin. The mouse monocytes – macrophages cells (J 774 A.1 cell line) with a high rate of non-specific uptake were cultured in DMEM, supplemented with 5% FBS at 37° C in a 5% CO_2 environment. To magnetically label cells, macrophages were

incubated in a suspension of Feridex I.V. solution diluted to 0.2 mgr/ml Fe. After 24 hours, cells were harvested and embedded into a mixture of 10% gelatin and 0.5% of silica particles acting as ultrasound scatterers. The mixture, was kept at 35ºC temperature, injected into a parenchyma of a fresh mouse kidney, and the sample was then cooled down to allow gel to harden. Prior to the imaging experiment, the kidney was positioned and fixed in a water cuvette.

C. *Pulsed magneto-acoustic imaging system*

A block diagram of the custom-built PMA imaging system is shown in Figure 1. A focused high-frequency single-element ultrasound transducer was used to capture ultrasound RF data. To obtain the images, the transducer was mechanically scanned over the region of interest. The magnetic field generator was based on a commercially available magnetic pulser (MPG5, SOTA, Inc.) but modified to meet the imaging system requirements. An iron-core was embedded into the coil in order to focus and maximize the magnetic field in the desired imaging region. The magnetic pulse strength, measured five mm above the iron-core tip using a digital gaussmeter (DSP 475, Lakeshore Inc.), was 0.6 Tesla. The focal point of ultrasound transducer and the iron-core tip were axially aligned to increase the magneto-acoustic sensitivity. The mechanical scanning was performed using a 2-D motion axes (x-y plane) attached to the water cuvette while the ultrasound transducer and the magnetic coil were kept fixed. A computer-based unit was utilized to control the positioning system, the ultrasound pulser and receiver, and the data acquisition unit. The cross-correlation approach was used to compute the displacement. Both B-scan ultrasound and magneto-acoustic images were reconstructed off-line.

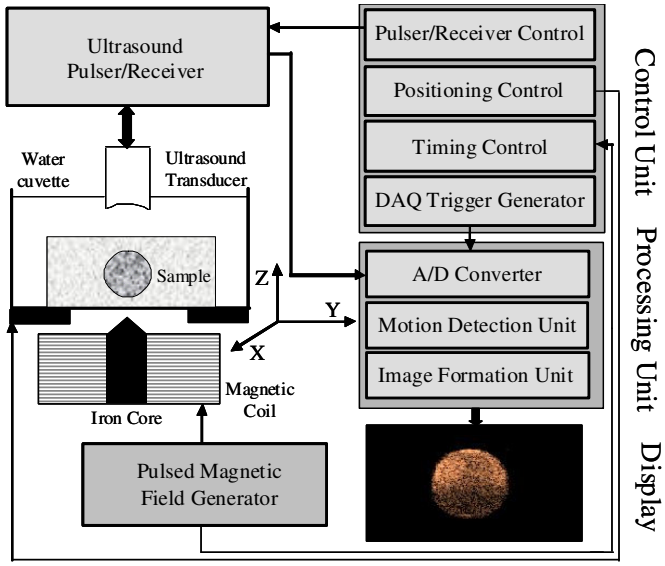

Fig. 1. Diagram of a custom-built PMA imaging system

Tissue mimicking phantoms were mechanically scanned with a 48 MHz single-element ultrasound transducer (focal depth = 5.5 mm, F# = 1.4) with 25 µm lateral steps. *Ex-vivo* experiments were performed using a 7.5 MHz single-element ultrasound transducer (focal depth = 50.8 mm, F# = 4) and the lateral steps were set to 200 µm.

The pulsed magneto-acoustic imaging system was designed to capture several pulse-echo signals before the application of the magnetic pulse. The pre-excitation RF lines were used as the reference to compute the relative displacement during the pulsed magnetic excitation as well as to reconstruct the B-scan ultrasound image. The relatively short magnetic pulses (6-10 ms) cause the iron-laden object to reach the maximum displacement in about 50 ms after the pulse. The high repetition frequency of ultrasound pulse-echo imaging was used to insure reliable measurement of the tissue displacement. Motion artifacts were eliminated by using the bottom of the water cuvette as a stationary reference – this reference motion was subtracted from the sample motion. The maximum displacement at each position within the imaging plane was then used to form the magneto-acoustic image.

IV. Results and Discussion

The B-scan ultrasound and magnetoacoustic images of the tissue-mimicking phantom are shown in Figure 2. Clearly, an ultrasound image cannot be used to differentiate between inclusions containing different concentrations of magnetic nano-agents. However, the magneto-acoustic image not only identifies the iron-laden inclusions, but also demonstrates the dependence of the PMA signal on the concentration of magnetic nano-agents.

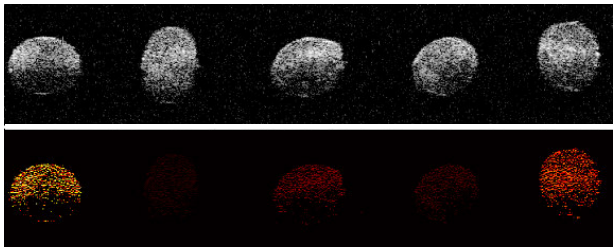

Fig. 2. a) B-scan ultrasound and b) magneto-acoustic images of phantoms with different concentrations of SPIO (left to right: 2.0, 0.0, 0.5, 0.2, and 1.0 mgr Fe/ml mixture). The field of view in both images is 18 mm by 3 mm

As a result of our calculations, the average displacements were found to be 45, 78, 215 and 330 µm for inclusions with 0.2, 0.5, 1.0 and 2.0 mgr Fe per ml concentration. The sensitivity of the current PMAI system can be improved further by increasing the magnetic excitation strength or by utilizing magnetic nanoparticles with higher susceptibility such as cobalt nanoparticles.

Figure 3 presents the results of PMA imaging of macrophage cells. The dark-field microscope image of the cells shows that cells contained iron-oxide nanoparticles. Although the ultrasound image (Fig. 3c) identifies the location of the gelatin inclusion within the background tissue, it is the combined ultrasound and magneto-acoustic

image (Fig. 3d) that clearly detects the presence of magnetically labeled cells within the tissue background.

The kidney tissue can be considered the control background with negligible magnetic susceptibility compared to the inclusion with magnetically labeled cells. The difference between the kidney and inclusion in B-scan ultrasound image is related to structural differences between those. However, the magneto-acoustic image shows the contrast between the inclusion and background tissue based on the presence of magnetically labeled tissue. Given the mechanical continuum, there is a small motion of the background tissue near the inclusion – the motion is reduced in regions that are farther away from the inclusion. The average displacement in the inclusion region was less than 50 µm. Although the displacement of the nanoparticles was reduced by the surrounding tissue, the results suggest that PMA imaging has a sensitivity to localize the magnetic nano-agents in tissue.

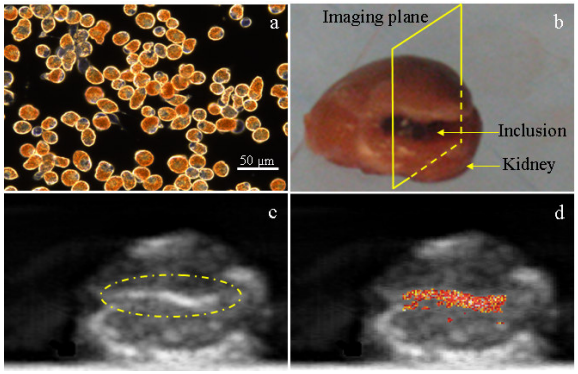

Fig. 3. (a) Optical dark-field reflectance image of murine macrophages labeled with SPIO, (b) Photograph of the kidney with gel inclusion containing magnetically labeled cells. The imaging plane is also shown here. (c) B-scan ultrasound image and (d) combined ultrasound and magneto-acoustic image of the kidney with inclusion.

The current imaging system is not capable of real-time imaging; and, therefore, post-processing was required to form both ultrasound and magneto-acoustic images. Real-time magneto-acoustic imaging is possible by utilizing a high frequency array-based ultrasound imaging system along with a modified magnetic field generator that provides a strong magneto-motive force in the imaging region. Furthermore, normalizing the tissue motion with respect to the magneto-motive force can provide more accurate information on the magnetic content of the tissue. In current ex-vivo experiments, the normalization was not performed because the background kidney tissue did not have significant magnetic properties compared to the inclusion.

In ex-vivo experiments, macrophage cells, incubated with nanoparticles, internalized a relatively high concentration of magnetic nanoparticles. However, the sensitivity of the PMA imaging system can be improved by adjusting several parameters such as nanoparticle magnetic properties and the magnetic excitation force. Consequently, magneto-acoustic imaging is suitable for in-vivo applications where magnetic nanoparticles are targeted to specific biomarkers. The fast motion of the iron-laden tissue can be separated from slowly-varying tissue motion in in-vivo applications.

V. Conclusion

The small size and non-toxicity of magnetic nanoparticles make them desired agents for imaging at the molecular and cellular level. Pulsed magneto-acoustic imaging was introduced as an imaging modality capable of detecting magnetically labeled tissue. The pulsed mode of operation allows for a higher magnetic field thus permitting the imaging of deeper tissue structures. Increasing the magneto-motive force and utilizing magnetic nano-agents with higher susceptibility can further improve the sensitivity of the system. In addition, with the development of biocompatible nanoparticles that have the desired molecular targeting moiety, magneto-acoustic imaging can become a molecular imaging technique capable of detecting pathology at early stages of development. Moreover, the dynamic behavior of magnetic nanoparticles represents the mechanical properties of the tissue and can be considered “remote palpation” for pathology specific imaging.

Acknowledgments

The authors are grateful to Mrs. Srivaleesha Mallidi (UT Austin) for helping with tissue experiments and Mr. Russell Torlage (SOTA Inc.) for technical help customizing the magnetic pulser. This work was partially supported by the National Institutes of Health under grant EB 008821.

References

[1] J. M. Correas, L. Bridal, A. Lesavre, A. Mejean, M. Claudon, and O. Helenon, "Ultrasound contrast agents: properties, principles of action, tolerance, and artifacts," *Eur Radiol*, vol. 11, pp. 1316-28, 2001.

[2] S. M. Demos, H. Alkan-Onyuksel, B. J. Kane, K. Ramani, A. Nagaraj, R. Greene, M. Klegerman, and D. D. McPherson, "In vivo targeting of acoustically reflective liposomes for intravascular and transvascular ultrasonic enhancement," *J Am Coll Cardiol*, vol. 33, pp. 867-75, 1999.

[3] W. G. Hundley, A. M. Kizilbash, I. Afridi, F. Franco, R. M. Peshock, and P. A. Grayburn, "Administration of an intravenous perfluorocarbon contrast agent improves echocardiographic determination of left ventricular volumes and ejection fraction: comparison with cine magnetic resonance imaging," *J Am Coll Cardiol*, vol. 32, pp. 1426-32, 1998.

[4] S. Mallidi, T. Larson, J. Aaron, K. Sokolov, and S. Emelianov, "Molecular specific optoacoustic imaging with plasmonic nanoparticles," *Optics Express*, vol. 15, pp. 6583-6588, 2007.

[5] M. Mehrmohammadi, J. Oh, L. Ma, E. Yantsen, T. Larson, S. Mallidi, S. Park, K. P. Johnston, K. Sokolov, T. Milner, and S. Emelianov, "Imaging of iron oxide nanoparticles using magneto-motive ultrasound," presented at Proceedings of the 2007 IEEE Ultrasonics Symposium, NY, 2007.

[6] J. F. Schenck, "Safety of strong, static magnetic fields," *J Magn Reson Imaging*, vol. 12, pp. 2-19, 2000.

[7] S. Wada, K. Tazawa, N. Suzuki, I. Furuta, and I. Nagano, "Pulp ablation therapy by inductive heating: heat generation characteristics in the pulp cavity," *Oral Dis*, vol. 13, pp. 193-7, 2007.

[8] S. R. Aglyamov, A. B. Karpiouk, Y. A. Ilinskii, E. A. Zabolotskaya, and S. Y. Emelianov, "Motion of a solid sphere in a viscoelastic medium in response to applied acoustic radiation force: Theoretical analysis and experimental verification," *J Acoust Soc Am*, vol. 122, pp. 1927-36, 2007.